Available online at www.sciencedirect.com
SCIENCE DIRECT®
Bioorganic & Medicinal Chemistry 13 (2005) 3691–3698
Bioorganic & Medicinal Chemistry

Comparison of positively charged DNG with DNA duplexes: a computational approach

Joseph W. Toporowski, Swarnalatha Y. Reddy and Thomas C. Bruice*

Department of Chemistry and Biochemistry, University of California, Santa Barbara, CA 93106, USA

Received 3 March 2005; accepted 14 March 2005
Available online 8 April 2005

Abstract—Molecular dynamics is used to investigate the structural properties of the cationic DNA analogue deoxynucleic guanidine (DNG), in which a guanidinium group replaces the phosphate moiety of DNA. This study examines the DNG duplex dodecamers $d(Ag)_{12}{\cdot}d(Tg)_{12}$ and $d(Gg)_{12}{\cdot}d(Cg)_{12}$, as well as their DNA counterparts. Watson–Crick base-pairing is maintained in the solvated DNG duplex models during the 5 ns simulations. The idealized DNG dodecamers assume many parameters characteristic of the corresponding native DNA, assuming B-DNA conformations. Several helical parameters are rather unique to DNG, including buckle, slide, inclination, propeller, and *X*-displacement. Fewer transitions in backbone torsions occur in the DNG duplexes compared to those of the DNA, which may result from the greater rigidity of the sp^2 hybridized guanidinium group verses the flexible sp^3 phosphate group. The DNG helices have exceptionally shallow major grooves and very deep minor grooves. The major and minor groove widths of DNG are narrower than those of the respective DNA counterparts.
© 2005 Elsevier Ltd. All rights reserved.

1. Introduction

In the search for effective antisense and antigene agents, much attention has focused on structural DNA analogues due to their potential to be highly sequence specific while maintaining binding affinity and resisting nuclease degradation. A common theme among many of these analogues involves preservation of the natural nucleobases while modifying the sugar rings and/or phosphodiester backbone to obtain a neutral single-strand, therefore increasing cellular uptake and eliminating the repulsion caused by two negatively charged strands. Many different structures have been explored, incorporating a wide range of chemistry. The aminoethyl glycal group of peptide nucleic acids completely replaces the phosphate and furanose moieties of natural oligonucleotides, creating a neutral species, which has shown high binding affinity for single-stranded DNA.[1] Replacement of the phosphodiester oxygens of DNA by sulfur, methyl groups, or amines yields analogues such as phosphorothiolates, methylphosphonates, and phosphoramidates, respectively.[2] Other backbone derivatives include acetals,[3] borano phosphates,[4] heterocycles,[5] locked nucleic acids,[6] methylene–methyliminos,[7] morpholinos,[8] and ureas.[9]

Deoxynucleic guanidine (DNG), in which a guanidinium group replaces the phosphodiester backbone of DNA (Fig. 1), has been designed to exploit DNA's natural negative charge by employing a cationic complementary strand, therefore enhancing duplex binding affinity while maintaining Watson–Crick base-pairing and specificity. Synthetic, thermal denaturation, binding, and exonuclease digestion studies have shown that DNG binds to complementary DNA strands with high

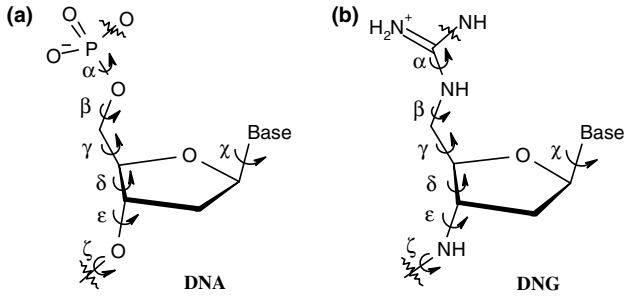

Figure 1. Repeating unit and torsional definitions of (a) DNA and (b) DNG.

Keywords: DNA analogue; Molecular dynamics; Guanidinium linkage; DNG.
* Corresponding author. Tel.: +1 805 893 2044; fax: +1 805 555 2229; e-mail: tcbruice@chem.ucsb.edu

0968-0896/$ - see front matter © 2005 Elsevier Ltd. All rights reserved.
doi:10.1016/j.bmc.2005.03.028

affinity and specificity and resists nuclease degradation.[10] Spectral observations of complementary DNG hexamers in solution suggest the formation of DNG duplexes with melting temperatures below 5 °C (similarly to DNA hexamers).[11]

Molecular dynamics (MD) has proven to be a powerful tool in elucidating structural and motion details of nucleic acids, proteins, and other biomolecules. Advances in force field development, the evaluation of long-range electrostatic interactions, and computing power have allowed for multi-nanosecond simulations incorporating explicit solvent and counterions.[12] While some limitations still exist (i.e., ion convergence, lack of polarizability due to semi-empirical force fields), the technology continues to become more reliable and predictive,[13] encouraging investigations into biomolecular properties that are difficult or inaccessible to study experimentally.

A-tracts, defined as a segment of DNA containing at least four sequential A base-steps, have been an intensely studied motif in nucleic acid research.[14–20] The combined results of X-ray crystallography, NMR, fiber diffraction, electrophoresis, and MD studies have elucidated the nature of the structure, hydration, and ionic properties of A-tracts. While A-tracts have been associated with local helix curvature,[14] crystallographic and MD studies have suggested that the A-tract itself is rigid and relatively straight[15] and the bending occurs at pyrimidine/purine steps adjacent to the A-tracts.[16,17] A-tracts assume structures associated with B-DNA and are characterized by a narrow minor groove,[18] high base-pair propeller,[19] and localized water spines.[19,20]

G-tracts, in contrast to A-tracts, have been shown to have wide minor grooves[21–23] and narrow major grooves,[24] the latter of which cationic activity is localized. Numerous experiments have established the tendency of G-tracts to undergo a B-DNA → A-DNA transition in solution.[24–28] This transition has been attributed to a decrease in water activity accompanied by an increase in cation occupation at the major groove.[29]

A previous MD study from this laboratory examined the structural properties of the DNA·DNG duplex $d(Ap)_8 \cdot d(Tg)_8$ and the DNG·DNA·DNG triplex $d(Tg)_8 \cdot d(Ap)_8 \cdot d(Tg)_8$.[30] The study concluded that Watson–Crick hydrogen bonds in both structures and Hoogstein hydrogen bonds in the triplex stayed intact. The structures assumed a mixed A/B-DNA form, showed a narrow minor groove and high propeller, and the combined anionic/cationic strands lead to a more compact structure compared to a DNA duplex.

This laboratory is in the process of studying DNG and its self-association, as the properties of such helices are important to understand. The structural features of idealized DNG·DNG duplex models $d(Ag)_{12} \cdot d(Tg)_{12}$ and $d(Gg)_{12} \cdot d(Cg)_{12}$ are examined in this study, including the stability of Watson–Crick base-pairing, backbone and base conformations, major and minor groove widths, and helical properties. The DNA equivalents of these dodecamers are also studied for comparison.

2. Methods

2.1. Setup

The CHARMM27 all-atom nucleic acid residue topology and parameter files[31,32] were used for the DNA simulations. Parameters for DNG were obtained based on similar structural groups found in amino acids (most notably arginine). The partial atomic charges (Table S1) of the DNG backbone were evaluated with the CHelpG option (Breneman scheme) at the MP2/6-311 + G(2d,p) level using GAUSSIAN03[33] for the model compound ethyl-*iso*-propyl-guanidinium (Fig. 2). The initial dodecamer structures $d(Ap)_{12} \cdot d(Tp)_{12}$ and $d(Gp)_{12} \cdot d(Cp)_{12}$ were constructed using the nucleic acid builder of QUANTA98,[34] selecting B-DNA as an initial conformer. Using QUANTA98, DNA was modified to the respective DNG molecule by replacing the phosphate groups (–O–(PO_2^-)–O–) with guanidinium groups (–NH–C(=N^+H_2)–NH–). The 5′-terminals of DNG were given amine groups, while hydroxyl groups were added to the 3′-terminals. Appropriate hydrogen atoms were built using QUANTA98. Sodium ions were added 5 Å away from the phosphorous atoms of DNA, while chloride ions were added 5 Å away from the guanidinium carbons of DNG to achieve neutral systems. The parameters for Na^+ and Cl^- are from the CHARMM27 forcefields.[31,32] These structures were energy minimized for 500 steps of steepest descent (SD) followed by 1000 steps of the adopted basis Newton–Raphson (ABNR) method using CHARMM (v. c27b4).[35]

2.2. MD details

The minimized systems were solvated in an orthorhombic box (44.67 Å × 64.06 Å × 43.74 Å) of 4116 pre-equilibrated TIP3P[36] water molecules. Solvent molecules that had an oxygen atom within 2.8 Å of a solute heavy atom were deleted, leaving 3691–3742 waters depending on the dodecamer. Periodic boundary conditions were applied. Images were generated using the CRYSTAL module of CHARMM. Electrostatic interactions were treated with the particle mesh Ewald method[37,38] as implemented in CHARMM,[39] using a real space cutoff of 10 Å

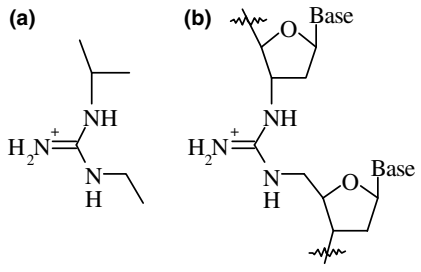

Figure 2. (a) Ethyl-*iso*-propyl-guanidinium used as a model compound to explore the partial charges of (b) a guanidinium linker between two DNG nucleotides.

(with Lennard–Jones interactions truncated at the same distance), a convergence parameter (κ) of 0.36 $Å^{-1}$, and a sixth degree B-spline interpolation. The solvent was then minimized for 100 SD steps and 1000 ABNR steps while the solute was kept fixed. All constraints were then released and the entire system was minimized for 2000 ABNR steps.

During dynamics, covalent bonds involving hydrogen atoms were constrained with SHAKE.[40] The leapfrog-Verlet algorithm[41] was used for integration with a time step of 1.5 fs. COM (center of mass) motion was not removed, as significant interaction with periodic images was not observed. Each simulation began by invoking harmonic constraints of 100 kcal mol^{-1} $Å^{-2}$ to all solute atoms, and letting the solvent equilibrate at 300 K for 30 ps under constant pressure and temperature conditions, allowing the dimensions of the water box to vary in all directions. Constraints on the counterions were then released, enabling them to equilibrate with the solvent for 15 ps under the same conditions. All constraints were then released and nuclear Overhauser effect (NOE) constraints were applied to the terminal base-pairs to reduce end base-pair fraying. (Simulations which were performed without the NOE constraints obtained similar results.) The entire system was allowed to equilibrate in 30 ps intervals at 125, 200, and 300 K. To achieve more stable trajectories,[42] constant volume and temperature (NVT) conditions were then invoked and the system continued to equilibrate for an additional 30 ps. After this initial 165 ps heating and equilibration period, the production stage was carried out until the total dynamics time reached 5 ns using the NVT ensemble.

2.3. Structural analyses

Root-mean-square deviations (rmsd) were based on all atoms excluding the terminal base-pairs. Evaluations of sugar puckers, nucleotide torsions, and intrastrand phosphate–phosphate ($P_n\cdots P_{n+1}$) and guanidinium carbon–carbon ($C_n\cdots C_{n+1}$) distances included the central eight base-pairs of each oligomer, while hydrogen bonding analysis excluded only terminal base pairs. Helical parameters were determined by use of FREEHELIX,[43] evaluating the central seven base steps and eight base-pairs of each dodecamer. Bending angles were defined as the angle between the normal vectors of base-pairs 3 and 10 of each duplex,[44,45] and were evaluated by use of FREEHELIX. Groove widths were defined as the distance between interstrand phosphorous atoms separated by three to four base-pairs, that is, $P(i-2)\cdots P'(i+2)$ across the major groove with four base-pair separation, and $P'(i-2)\cdots P(i+2)$ across the minor groove with three base-pair separation.[44] In the case of DNG, guanidinium carbons were used in place of phosphorous atoms (Fig. 1). Canonical A and B-DNA structures were generated with QUANTA98 for comparison purposes. Average structures were obtained by a least squares fitting of all oligomer atoms saved at 0.75 ps intervals from the trajectories to the minimized structure. These averaged structures were minimized for 500 steps of SD, and the corresponding stereo plots were produced using MidasPlus.[46,47] The solvent-accessible surface area (SASA) was estimated according to Lee and Richards[48] with a water probe radius of 1.4 Å. The SASA around the major groove was evaluated by considering atoms N6 of adenine, O6 of guanine, O4 of thymine, and N4 of cytosine; the minor groove by selecting N3 of adenine, N3 and N2 of guanine, and O2 of the pyrimidines;[49] the guanidinium group by selecting atoms CG1, NG1, HG11, and HG12 (Fig. S1); and the phosphate group by selecting atoms P, O1P, and O2P.

3. Results and discussion

3.1. $d(A)_{12}\cdot d(T)_{12}$

3.1.1. Rmsd. The root-mean-square deviations (rmsd) of the DNG and DNA atoms with respect to the minimized structures and canonical A-DNA and B-DNA forms are given in Figure 3a. The values for the $d(Ag)_{12}\cdot d(Tg)_{12}$ complex with respect to the minimized structure range from 2.44 to 5.21 Å (red) and similarly to the canonical B-DNA form (blue). The deviations are high (7.35–9.70 Å) compared to canonical A-DNA (green), remaining about twice the distance compared to the minimized structure. A simulation of $d(Ag)_{12}\cdot d(Tg)_{12}$ undertaken with a different initial conformation

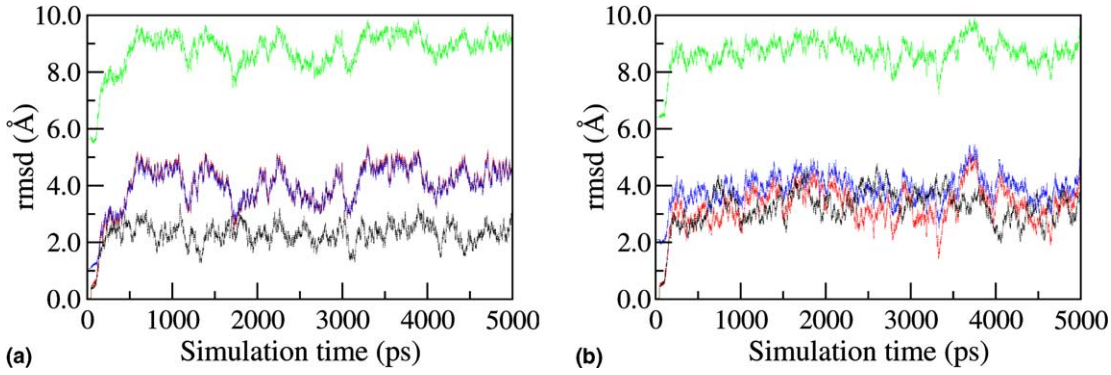

Figure 3. Time variation plots of rmsd for (a) $d(A)_{12}\cdot d(T)_{12}$ and (b) $d(G)_{12}\cdot d(C)_{12}$. Shown are the DNA values with respect to minimized DNA (black), and DNG values with respect to minimized DNG (red), canonical A-DNA (green), and canonical B-DNA (blue). Note that the red and blue lines overlap in (a).

(canonical A-DNA) also leads to a B-type structure, with the A → B-DNA transition occurring around 1 ns (rmsd plot given in Fig. S2). The corresponding DNA structure $d(Ap)_{12}{\cdot}d(Tp)_{12}$ shows low values ranging 1.28–3.37 Å from its minimized structure (black). The magnitude of these deviations is not surprising, considering that minor changes in helical and structural parameters can lead to relatively large rmsd values in nucleic acid simulations, as explained by Cheatham and Kollman.[49]

3.1.2. Watson–Crick base pairing. The Watson–Crick hydrogen bonds remain intact throughout the simulations. For both DNG and DNA duplexes, the N1···N3 distance (2.9 ± 0.1 Å) stays tighter than the N6···O4 distance (3.0 ± 0.2 Å). While DNA duplex melting occurs on time scales in the microsecond to millisecond range,[50,51] it is likely that significant geometric or steric barriers to DNG duplex stability would lead to quicker melting periods. The results of this simulation suggest that such barriers do not exist to the extent that melting is not observed in the low nanosecond range. This helps to support the spectral data, which suggests a 1:1 complexation of complementary DNG hexamers.[11]

3.1.3. Sugar pucker. Figures 4 and S2 give stereo views of $d(A)_{12}{\cdot}d(T)_{12}$ helices in which structural differences between DNG and DNA can be observed. The sugar pucker values obtained for both the $d(Ag)_{12}{\cdot}d(Tg)_{12}$ and $d(Ap)_{12}{\cdot}d(Tp)_{12}$ structures are in the C2′-*endo* region (155 ± 15°). These values are similar to those reported in fiber diffraction studies of poly(dAp)·poly(dTp).[18,52] However, while the DNG favors C2′-*endo*, the DNA simulation shows transitions from C2′-*endo* to C3′-*endo* (20 ± 15°), which generally last for about 150 ps, but can last up to 370 ps. MD studies on $d(Ap)_{30}{\cdot}d(Tp)_{30}$[17] and the A-tract regions of $d(CGCGA_6CG)$ and $d(CGCA_6GCG)$[19] report sugar puckering values of C1′-*exo* (~130° for the A-strand and ~115° for the T-strand).

3.1.4. Backbone and glycosyl conformations. The transitions between B-DNA substates have been suggested to play a role in complex formation and biological function, as reviewed by Winger et al.[53] The B-DNA substates B_I and B_{II} are defined by torsions ε (C4′–C3′–O3′–P) and ζ (C3′–O3′–P–O5′) of the sugar–phosphate backbone. This definition is applied to DNG, with torsions defined by ε (C4′–C3′–NG3–CG1) and ζ (C3′–NG3–CG1–NG5) (Figs. 1 and S1). Throughout the course of the $d(Ag)_{12}{\cdot}d(Tg)_{12}$ simulation, both the A_{12} and T_{12} strands have ε values, which generally favor a *trans* (208 ± 12°) conformation, but fluctuations in the T strand to *gauche*$^-$ (260 ± 15°) last up to 250 ps. ζ holds steady as *trans* (175 ± 11°). Conformer B_I is characterized by ε and ζ values of *trans* (120–210°) and *gauche*$^-$ (235–295°), respectively, while the B_{II} conformer corresponds to ε and ζ values of *gauche*$^-$ (210–300°) and *trans* (150–210°).[53] Based on these definitions and the values ε and ζ from MD, the DNG duplex exists closer to the B_{II} conformer designation. Torsion α (NG3–CG1–NG5–C5′) remains *gauche*$^-$ (355 ± 12°), and γ (NG5–C5′–C4′–C3′) prefers *gauche*$^+$ (67 ± 8°). The glycosyl torsion χ (O4′–C1′–N1–C2 for pyrimidines, O4′–C1′–N9′–C4 for purines) adopts a high *anti* (273 ± 11°) conformation. The backbone of three $d(Ag)_{12}{\cdot}d(Tg)_{12}$ nucleotides is shown in Figure 5.

B_I conformations are observed during the $d(Ap)_{12}{\cdot}d(Tp)_{12}$ simulation, with ε favoring a *trans* (188 ± 10°) conformation in both strands and brief (<20 ps) spikes to *gauche*$^-$ (270°) seen in some A nucleotides (Fig. S2). ζ is typically *gauche*$^-$ (255 ± 15°), with occasional spikes to *trans* (150°) and more extended fluctuations to a higher *gauche*$^-$ (290 ± 15°), lasting up to 370 ps. Torsion α (O3′–P–O5′–C5′) remains *gauche*$^-$ (300 ± 14°), while γ (NG5–C5′–C4′–C3′) prefers *gauche*$^+$ (51 ± 13°). Glycosyl χ is observed to be *anti* (253 ± 12° with transitions to 210 ± 10° lasting up to 370 ps) in both A and T nucleotides. These results are consistent with X-ray diffraction studies[54] of poly(dAp)·poly(dTp), which are: ε 145.3°, ζ 273.1°, α 307.1°, γ 39.4°, and χ as 144.5°.

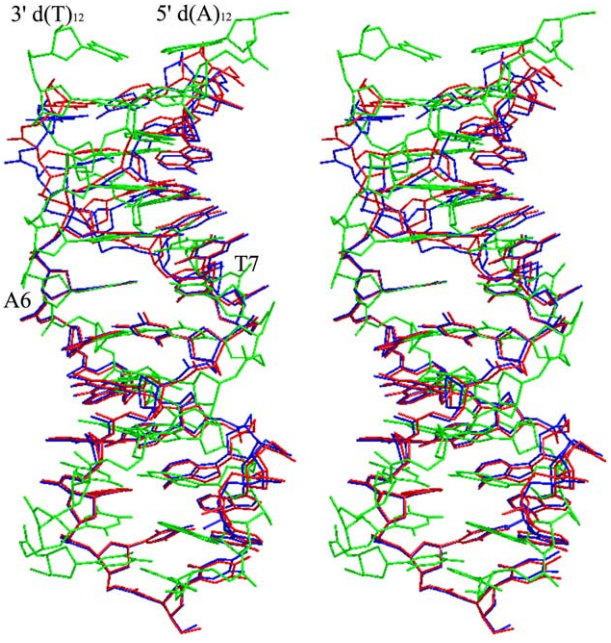

Figure 4. Stereo view of the $d(Ag)_{12}{\cdot}d(Tg)_{12}$ helix. Superimposed are the minimized (green), 2–3 ns (red), and 4–5 ns (blue) averaged MD structures.

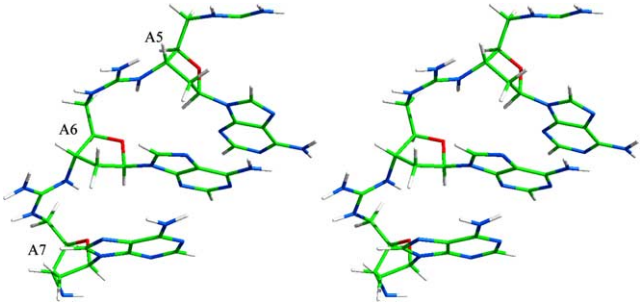

Figure 5. Stereo view of the guanidinium backbone in nucleotides A5–A7 of the MD averaged (2–3 ns) $d(Ag)_{12}{\cdot}d(Tg)_{12}$ structure.

3.1.5. Groove widths. The major and minor groove widths are given in Table S2. The major groove width for $d(Ag)_{12}\cdot d(Tg)_{12}$ varies around 17.0 ± 0.7 Å, while the minor groove width demonstrates less steadiness with values of 11.3 ± 1.2 Å. The major groove width of $d(Ap)_{12}\cdot d(Tp)_{12}$ adopts a range of 17.6 ± 1.6 Å, and the minor groove width is 13.1 ± 1.1 Å. Both the DNG and DNA grooves widths are characteristic of canonical B-DNA, which has major and minor grooves widths of 17.3 and 11.5 Å, respectively. However, the DNG minor groove shows a trend of gradually getting wider toward the central base pairs and narrowing further down the helix. The grooves of the $d(A)_{12}\cdot d(T)_{12}$ helices can be seen in stereo in Figure 6. From Figure 6a, it is apparent that the DNG minor groove is narrow and deep, while the major groove is extremely shallow. The guanidinium groups (colored yellow and pink) can be seen to partially orient into the major groove, similarly to the phosphates of DNA (Fig. 6b).

3.1.6. Intrastrand phosphate–phosphate distances. The DNA intrastrand ($P_n\cdots P_{n+1}$) distances are evaluated and compared to the intrastrand guanidinium carbon–carbon ($C_n\cdots C_{n+1}$) distances of DNG. The DNA values of 6.8 ± 0.2 Å tend to be slightly longer than those of the DNG, which are measured at 6.7 ± 0.2 Å. This difference may at least partially be accounted for by the fact that the sp^2 hybridized guanidinium carbons will contract the distances between the adjacent nucleotides more than the tetrahedral geometry of the sp^3 phosphate groups.

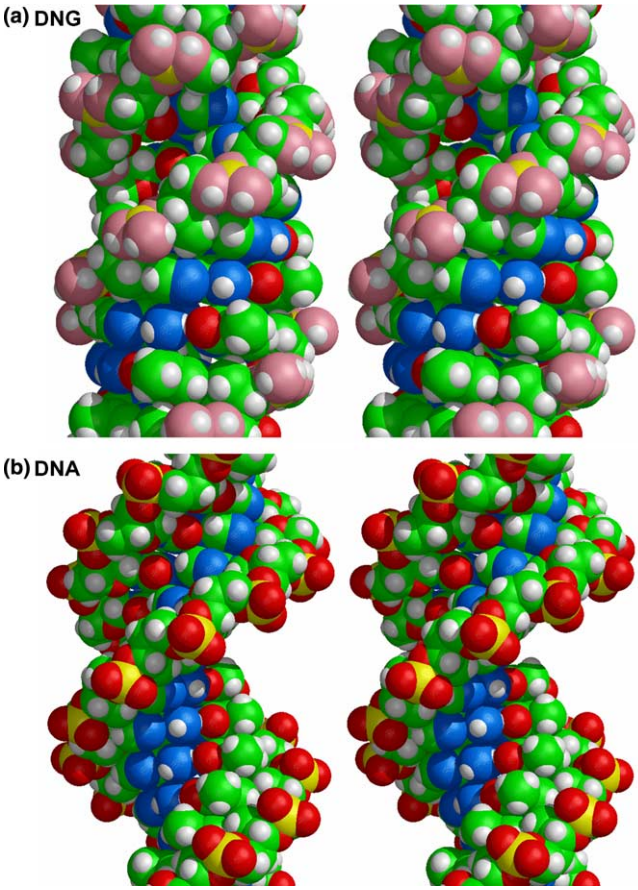

Figure 6. CPK stereo models of (a) $d(Ag)_{12}\cdot d(Tg)_{12}$ and (b) $d(Ap)_{12}\cdot d(Tp)_{12}$ MD averaged (4–5 ns) structures. In (a) the guanidinium carbons and nitrogens are yellow and pink, respectively, and in (b) the phosphorous atoms are yellow.

3.1.7. Solvent-accessible surface area (SASA). Investigations of the $d(A)_{12}\cdot d(T)_{12}$ duplexes show ~350 Å less SASA around the guanidinium groups of DNG compared to the phosphates of DNA (Fig. S6a). This disparity may be an effect of the different geometries of the functional groups, and could also be due to differences in the oppositely charged functional groups' ability to form hydrogen bonds with water. The major groove SASA values of the DNG remain ~400 $Å^2$ above those of the DNA (Fig. S6b). In contrast, the minor groove SASA shows similar trends between the analogues, with DNG values ~50 $Å^2$ larger than those of the DNA duplexes (Fig. S6c).

3.1.8. Helix bending. Time variation plots for the A-tract helical bending angles are given in Figure 7a. Slightly more helical bending (~4°) is observed in the $d(Ag)_{12}\cdot d(Tg)_{12}$ duplex (19 ± 10°) than in the $d(Ap)_{12}\cdot d(Tp)_{12}$ helix (15 ± 7°).

3.1.9. Helical parameters. The helical parameters for $d(Ag)_{12}\cdot d(Tg)_{12}$, $d(Ap)_{12}\cdot d(Tp)_{12}$, and canonical DNA are given in Table 1. The $d(Ag)_{12}\cdot d(Tg)_{12}$ helix demonstrates negative roll (−11 ± 10°), accompanied by negative tilt (−8 ± 4°) and high twist (42 ± 3°). Each of these rotational base-step parameters is more similar to B-DNA than to A-DNA. The oligonucleotide displays positive translational base-step parameters, but while the rise values (3.3 ± 0.3 Å) are characteristic of B-DNA, the large slide values (2.4 ± 0.7 Å) are substantially higher than either canonical form of DNA.

As for the rotational base-pair values of $d(Ag)_{12}\cdot d(Tg)_{12}$, a significant amount of positive tip (12 ± 8°) is observed, as is sizable negative inclination (−14 ± 5°), and negative buckle (−11 ± 6°). An exceptionally negative propeller (−30 ± 11°) is observed, and although this value is well below canonical B-DNA (−1°), large negative propeller values are characteristic of A-tracts.[17,55] While none of these values are characteristic of canonical DNA, they are each closer to B-DNA than to A-DNA. Translational base-pair term *X*-displacement is high (3.6 ± 1.2 Å). The base-step parameters for the DNA exhibit B-DNA-like characteristics in agreement with experimental results, which show that A-tracts assume a B-DNA form. The base-pair parameters, however, show more deviations from canonical B-DNA form. The parameters are in excellent agreement with MD studies on A-tracts as reported by McConnell and Beveridge.[17]

3.2. $d(G)_{12}\cdot d(C)_{12}$

3.2.1. Rmsd. Figure 3b shows the collected rmsds for $d(Gg)_{12}\cdot d(Cg)_{12}$ with respect to its minimized structure (red) and canonical A (green) and B (blue) forms. The rmsd of the $d(Gg)_{12}\cdot d(Cg)_{12}$ helix ranges 2.09–4.54 Å

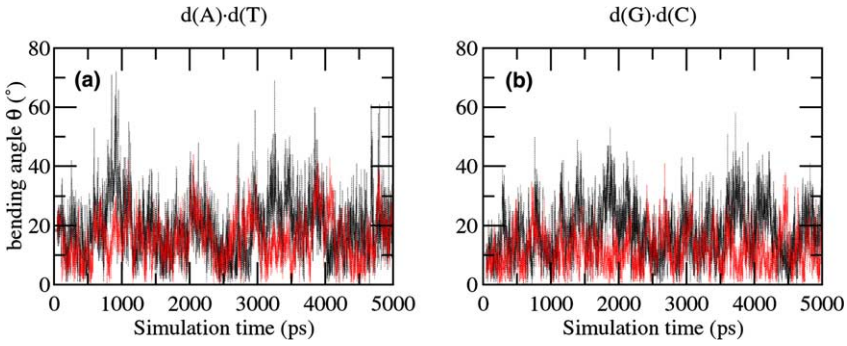

Figure 7. Bending angles of (a) $d(A)_{12}\cdot d(T)_{12}$ and (b) $d(G)_{12}\cdot d(C)_{12}$ helices for DNG (black) and DNA (red).

Table 1. Helical parameters (with standard deviations) of the MD averaged DNG and DNA structures and canonical DNA

	$d(A)_{12}\cdot d(T)_{12}$		$d(G)_{12}\cdot d(C)_{12}$		Canonical DNA	
	DNG	DNA	DNG	DNA	A	B
Roll (°)	−11 ± 10	4 ± 5	−9 ± 8	2 ± 5	11	−3
Tilt (°)	−8 ± 4	−3 ± 3	−3 ± 4	0 ± 2	1	0
Twist (°)	42 ± 3	35 ± 4	40 ± 3	33 ± 5	33	36
Rise (Å)	3.3 ± 0.3	3.2 ± 0.4	3.4 ± 0.3	3.3 ± 0.4	2.3	3.4
Slide (Å)	2.4 ± 0.7	−0.3 ± 0.5	2.9 ± 0.5	−0.9 ± 0.5	−1.6	−0.2
Tip (°)	12 ± 8	4 ± 4	5 ± 7	−1 ± 4	−1	0
Inclination (°)	−14 ± 5	6 ± 5	−12 ± 5	3 ± 4	20	−5
Propeller (°)	−30 ± 11	−13 ± 7	−24 ± 10	2 ± 8	11	−1
Buckle (°)	−11 ± 6	−4 ± 10	−10 ± 6	0 ± 9	0	0
X-Displacement (Å)	3.6 ± 1.2	−1.4 ± 0.8	4.1 ± 1.0	−2.1 ± 1.0	−4.5	0.2

from its minimized structure, and 0.5–1.0 Å higher with respect to canonical B form. The values are substantially higher for canonical A form (~5 Å larger). The rmsd of $d(Gp)_{12}\cdot d(Cp)_{12}$ (black) ranges 2.34–4.78 Å from its minimized structure, generally staying lower than the DNG duplex.

3.2.2. Sugar pucker. Stereo views of the $d(G)_{12}\cdot d(C)_{12}$ MD averaged structures are given in Figures S3 and S4. The sugar puckering observed for both $d(Gp)_{12}\cdot d(Cp)_{12}$ and $d(Gg)_{12}\cdot d(Cg)_{12}$ lies in the C2′-*endo* (155 ± 12°) region. The DNG sugars remain steady while the DNA sugars demonstrate transitions to C3′-*endo* (20 ± 10°). The transitions are seen in each DNA nucleotide, the longest of which remains in the C3′-*endo* domain for 460 ps.

3.2.3. Backbone and glycosyl conformations. No significant transitions in backbone torsions for $d(Gg)_{12}\cdot d(Cg)_{12}$ are seen during the 5 ns simulation. *trans* Values of ε (213 ± 14°) and ζ (172 ± 11°) that correspond to the B_{II} conformer are observed. Torsion α favors *gauche*$^-$ (355 ± 13°) and γ prefers *gauche*$^+$ (65 ± 8°). The glycosyl torsion χ stays in a high *anti* (277 ± 10°) conformation. Watson–Crick hydrogen bonding is maintained for both $d(Gg)_{12}\cdot d(Cg)_{12}$ and $d(Gp)_{12}\cdot d(Cp)_{12}$ throughout the simulations.

The oligonucleotide $d(Gp)_{12}\cdot d(Cp)_{12}$ adopts a B_I conformation during dynamics. *trans* Values of ε (188 ± 11°) are observed, but brief (<95 ps) jumps to *gauche*$^-$ (260 ± 10°) occur. ζ generally prefers *gauche*$^-$ (257 ± 14°), although for some extended periods values of higher *gauche*$^-$ (290 ± 15°) are observed for up to 460 ps, as are some brief (<80 ps) transitions to *trans* (170 ± 15°). Throughout the simulation, α assumes a *gauche*$^-$ (298 ± 15°) conformation and γ prefers *gauche*$^+$ (51 ± 13°). Glycosyl χ typically stays *anti* (245 ± 16°), but shifts to a lower *anti* (200 ± 10°) lasting up to 750 ps are also observed.

3.2.4. Groove widths. Both the major and minor groove widths are narrower for the DNG than the DNA (Table S2). The major groove of $d(Gg)_{12}\cdot d(Cg)_{12}$ holds steady at 16.7 ± 0.7 Å, while the minor groove is typically 13.1 ± 1.4 Å. These values are more similar to canonical B-DNA (17.3 Å major groove and 11.5 Å minor groove) than to the A-DNA form (8.3 Å major groove and 17.4 Å minor groove). The values for the $d(Gp)_{12}\cdot d(Cp)_{12}$ major groove vary in the 18.9 ± 1.7 Å region, comparable to B-DNA. The DNA minor groove width lies between canonical values at 14.0 ± 1.1 Å. Although the DNG major groove is narrower than that of the DNA, neither duplex possesses a distinctly narrow major groove as is known to occur in G-tracts.[24] However the DNA G-tract does have a wide minor groove compared to canonical B-DNA, a trait which has been previously reported.[21–23] The DNG minor groove demonstrates a trend of widening toward the middle of the helix and narrowing towards the ends. Figure S4 gives CPK stereo views of the $d(G)_{12}\cdot d(C)_{12}$ helices, in which the DNG can be seen to have a deep minor groove and very shallow major groove. Figure S4a shows the guanidinium groups adopting a similar

conformation to the phosphates of DNA (Fig. S4b), orientating into the major groove.

3.2.5. Intrastrand phosphate–phosphate distance. The intrastrand guanidinium carbon–carbon distances of the DNG duplex are very similar to the intrastrand $P_n\cdots P_{n+1}$ distances. The guanidinium $C_n\cdots C_{n+1}$ distances observed for DNG are 6.6 ± 0.2 Å, while the $P_n\cdots P_{n+1}$ distances of the DNA simulation are 6.7 ± 0.3 Å. No distinct variations in DNG distances are observed, but transitions to more constricted values of 6.0 ± 0.3 Å (extending up to 420 ps) are noticed for some DNA $P_n\cdots P_{n+1}$ distances.

3.2.6. SASA. Analysis of the $d(G)_{12}\cdot d(C)_{12}$ duplexes shows ~350 Å^2 more SASA around the phosphate groups compared to the guanidinium groups (Fig. S6d). The SASA of the major grooves shows DNG values 375 Å^2 larger than those of the DNA (Fig. S6e). Minor groove levels are very similar between the analogues, with the DNA values ~25 Å^2 larger than those of the DNG (Fig. S6f).

3.2.7. Helix bending. The plots for helical bending are given in Figure 7b. While the $d(Gp)_{12}\cdot d(Cp)_{12}$ duplex remained bent by 12 ± 6°, the DNG displayed slightly more tendency to bend, with average values of 18 ± 9°.

3.2.8. Helical parameters. The DNG oligomer assumes rotational base-step parameters of negative roll (−9 ± 8°) similar to B-DNA, tilt values (−3 ± 4°) slightly lower than both canonical forms, and twist values (40 ± 3°) similar to B-DNA (Table 1). Positive translational base-step parameters are demonstrated, with B-DNA-like rise values (3.4 ± 0.3 Å) and very high values of slide (2.9 ± 0.5 Å). Rotational base-pair parameters inclination (−12 ± 5°), propeller (−24 ± 10°), and buckle (−10 ± 6°) lie moderately below canonical B-DNA values. The adopted positive tip (5 ± 7°) is larger than both canonical forms, as is the translational base-pair parameter *X*-displacement, which is considerably high (4.1 ± 1.0 Å). The DNA sequence $d(Gp)_{12}\cdot d(Cp)_{12}$ assumes some helical parameters, which lie between canonical values, but altogether which lie closer to B-DNA. These results are in accord with previous MD G-tract studies.[17]

4. Conclusions

The 5 ns MD studies show that under the applied simulation conditions, models of DNG dodecamers $d(Ag)_{12}\cdot d(Tg)_{12}$ and $d(Gg)_{12}\cdot d(Cg)_{12}$ maintain Watson–Crick base pairing in an aqueous environment while adopting a form similar to canonical B-DNA. Lending credence to the DNG analysis are the results of the corresponding DNA duplexes, which are in accord with results presented in previous MD[17,19] and experimental studies.[18,52]

Several trends are seen in the comparison of DNG and DNA duplexes. The rmsds of the DNG duplexes tend to be larger than those of DNA. The DNG helices display less variations in sugar pucker, backbone, and glycosyl torsion than the DNA. This pattern of less deviation in the DNG parameters compared to DNA may be a direct result of the higher rigidity of the sp^2 hybridized guanidinium group versus the flexible sp^3 hybridized phosphate group of DNA. This difference in backbone flexibility may also account for slightly shorter intrastrand guanidinium carbon distances of DNG compared to the intrastrand phosphate distances of DNA. Both DNG helices favor the B_{II} substate, while the DNA counterparts prefer B_I. As can be seen in Figure 1, the atoms and hybridization states that constitute torsions ε and ζ are not the same between the two analogues. Therefore the properties of these substates, such as the increased base-stacking interactions of the B_I substate,[53,56] may be associated with different ε and ζ ranges for DNA and DNG.

The simulations show more bending in the DNG helices than in the DNA (Fig. 7). No B-DNA → A-DNA transitions are seen in either G-tract simulation, however the DNA analogue does assume some A-DNA like helical parameters, as has been observed in previous MD studies.[24–28] The DNG guanidinium groups demonstrate lower SASA values than the phosphates of DNA, while the DNG major grooves show higher levels than the DNA, and the minor grooves show similar SASA trends to each other (Fig. S6). The DNG duplexes also display some unique helical parameters with low buckle, inclination, and propeller values, and large slide and *X*-displacement values.

Major and minor groove widths of each duplex are characteristic of B-DNA, with the exception of the $d(Gp)_{12}\cdot d(Cp)_{12}$ minor groove which lies between canonical A- and B-DNA values. Both major and minor groove widths are narrower in the DNG than the DNA. DNG is shown to have exceptionally shallow major grooves and deep minor grooves. The guanidinium groups of DNG orient into the major groove, as do the phosphate groups of DNA.

In both the DNG and DNA simulations, the A-tracts remain slightly straighter than the G-tracts. The minor grooves of the A-tracts tend to be narrower than those of the G-tracts. Most other parameters are similar between the A- and G-tracts, with a notable exception being that the G-tracts prefer several helical parameters that are either characteristic of or close to A-DNA.

Acknowledgements

J.T. thanks and is grateful to Dr. Jia Luo for an invaluable introduction to the concepts and execution of molecular dynamics. Support for this study has been provided by the NIH Grant 5R37DK0917136.

Supplementary data

Supplementary data associated with this article can be found, in the online version at doi:10.1016/j.bmc.2005.03.028.

References and notes

1. Egholm, M.; Buchardt, O.; Nielsen, P. E.; Berg, R. H. *J. Am. Chem. Soc.* **1992**, *114*, 1895.
2. De Mesmaeker, A.; Altmann, K.; Waldner, A.; Wendeborn, S. *Curr. Opin. Struct. Biol.* **1995**, *5*, 343.
3. Wang, J.; Matteucci, M. D. *Bioorg. Med. Chem. Lett.* **1997**, *7*, 229.
4. Sood, A.; Shaw, B. R.; Spielvogel, B. F. *J. Am. Chem. Soc.* **1990**, *112*, 9000.
5. von Matt, P.; Altmann, K. H. *Bioorg. Med. Chem. Lett.* **1997**, *7*, 1553.
6. Kurreck, J.; Wyszko, E.; Gillen, C.; Erdmann, V. A. *Nucleic Acids Res.* **2002**, *30*, 1911.
7. Morvan, F.; Sanghvi, Y. S.; Perbost, M.; Vasseur, J.; Bellon, L. *J. Am. Chem. Soc.* **1996**, *118*, 225.
8. Summerton, J.; Weller, D. *Nucleosides Nucleotides* **1997**, *16*, 889.
9. Waldner, A.; De Mesmaeker, A.; Lebreton, J.; Fritsch, V.; Wolf, R. M. *Synlett* **1994**, *1*, 57.
10. Barawkar, D. A.; Bruice, T. C. *Proc. Natl. Acad. Sci. U.S.A.* **1998**, *95*, 11047.
11. Reddy, P. M.; Bruice, T. C. *Bioorg. Med. Chem. Lett.* **2003**, *13*, 1281.
12. Norberg, J.; Nilsson, L. *Q. Rev. Biophys.* **2003**, *36*, 257.
13. Cheatham, T. E., III. *Curr. Opin. Struct. Biol.* **2004**, *14*, 360.
14. Marini, J. C.; Levene, S. D.; Crothers, D. M.; Englund, P. T. *Proc. Natl. Acad. Sci. U.S.A.* **1982**, *79*, 7664.
15. Dickerson, R. E.; Goodsell, D.; Kopka, M. L. *J. Mol. Biol.* **1996**, *256*, 108.
16. Beveridge, D. L.; Dixit, S. B.; Barreiro, G.; Thayer, K. M. *Biopolymers* **2004**, *73*, 380.
17. McConnell, K. J.; Beveridge, D. L. *J. Mol. Biol.* **2001**, *314*, 23.
18. Alexeev, D. G.; Lipanov, A. A.; Skuratovskii, I. Y. *Nature* **1987**, *325*, 821.
19. Strahs, D.; Schlick, T. *J. Mol. Biol.* **2000**, *301*, 643.
20. Drew, H. R.; Dickerson, R. E. *J. Mol. Biol.* **1981**, *151*, 535.
21. Dornberger, U.; Leijon, M.; Fritzsche, H. *J. Biol. Chem.* **1999**, *274*, 6957.
22. Heinemann, U.; Alings, C. *J. Mol. Biol.* **1989**, *210*, 369.
23. Heinemann, U.; Alings, C.; Bansal, M. *EMBO J.* **1992**, *11*, 1931.
24. Hud, N. V.; Plavec, J. *Biopolymers* **2003**, *69*, 144.
25. Early, T. A.; Kearns, D. R.; Burd, J. F.; Larson, J. E.; Wells, R. D. *Biochemistry* **1977**, *16*, 541.
26. Nishimura, Y.; Torigoe, C.; Tsuboi, M. *Biopolymers* **1985**, *24*, 1841.
27. Nishimura, Y.; Torigoe, C.; Tsuboi, M. *Nucleic Acids Res.* **1986**, *14*, 2737.
28. Xu, Q.; Shoemaker, R. K.; Braunlin, W. H. *Biophys. J.* **1993**, *65*, 1039.
29. Cheatham, T. E., III; Kollman, P. A. *Structure* **1997**, *5*, 1297.
30. Luo, J.; Bruice, T. C. *J. Am. Chem. Soc.* **1998**, *120*, 1115.
31. MacKerell, A. D., Jr.; Bashford, D.; Bellott, M.; Dunbrack, R. L.; Evanseck, J. D.; Field, M. J.; Fischer, S.; Gao, J.; Guo, H.; Ha, S.; Joseph-McCarthy, D.; Kuchnir, L.; Kuczera, K.; Lau, F. T. K.; Mattos, C.; Michnick, S.; Ngo, T.; Nguyen, D. T.; Prodhom, B.; Reiher, W. E.; Roux, B.; Schlenkrich, M.; Smith, J. C.; Stote, R.; Straub, J.; Watanabe, M.; Wiórkiewicz-Kuczera, J.; Yin, D.; Karplus, M. *J. Phys. Chem. B* **1998**, *102*, 3586.
32. MacKerell, A. D.; Banavali, N. *J. Comput. Chem.* **2000**, *21*, 105.
33. Frisch, M. J.; Trucks, G. W.; Schlegel, H. B.; Scuseria, G. E.; Robb, M. A.; Cheeseman, J. R.; Montgomery, J. A., Jr.; Vreven, T.; Kudin, K. N.; Burant, J. C.; Millam, J. M.; Iyengar, S. S.; Tomasi, J.; Barone, V.; Mennucci, B.; Cossi, M.; Scalmani, G.; Rega, N.; Petersson, G. A.; Nakatsuji, H.; Hada, M.; Ehara, M.; Toyota, K.; Fukuda, R.; Hasegawa, J.; Ishida, M.; Nakajima, T.; Honda, Y.; Kitao, O.; Nakai, H.; Klene, M.; Li, X.; Knox, J. E.; Hratchian, H. P.; Cross, J. B.; Adamo, C.; Jaramillo, J.; Gomperts, R.; Stratmann, R. E.; Yazyev, O.; Austin, A. J.; Cammi, R.; Pomelli, C.; Ochterski, J. W.; Ayala, P. Y.; Morokuma, K.; Voth, G. A.; Salvador, P.; Dannenberg, J. J.; Zakrzewski, V. G.; Dapprich, S.; Daniels, A. D.; Strain, M. C.; Farkas, O.; Malick, D. K.; Rabuck, A. D.; Raghavachari, K.; Foresman, J. B.; Ortiz, J. V.; Cui, Q.; Baboul, A. G.; Clifford, S.; Cioslowski, J.; Stefanov, B. B.; Liu, G.; Liashenko, A.; Piskorz, P.; Komaromi, I.; Martin, R. L.; Fox, D. J.; Keith, T.; Al-Laham, M. A.; Peng, C. Y.; Nanayakkara, A.; Challacombe, M.; Gill, P. M. W.; Johnson, B.; Chen, W.; Wong, M. W.; Gonzalez, C.; Pople, J. A., Gaussian 03, Revision B.05; Gaussian, Inc., Pittsburgh PA, 2003.
34. QUANTA98; Molecular Simulation Inc.: San Diego, CA, 1998.
35. Brooks, B. R.; Bruccoleri, R. E.; Olafson, B. D.; States, D. J.; Swaminathan, S.; Karplus, M. *J. Comput. Chem.* **1983**, *4*, 187.
36. Jorgensen, W. L.; Chandrasekhar, J.; Madura, J. D.; Impey, R. W.; Klein, M. L. *J. Chem. Phys.* **1983**, *79*, 926.
37. Darden, T.; York, D.; Pedersen, L. *J. Chem. Phys.* **1993**, *98*, 10089.
38. Petersen, H. G. *J. Chem. Phys.* **1995**, *103*, 3668.
39. Feller, S. E.; Pastor, R. W.; Rojnuckarin, A.; Bogusz, S.; Brooks, B. R. *J. Phys. Chem.* **1996**, *100*, 17011.
40. Ryckaert, J. P.; Ciccotti, G.; Berendsen, H. J. C. *J. Comput. Phys.* **1977**, *23*, 237.
41. Verlet, L. *Phys. Rev.* **1967**, *159*, 98.
42. Brown, D.; Clarke, J. H. R. *Mol. Phys.* **1984**, *51*, 1243.
43. Dickerson, R. E. *Nucleic Acids Res.* **1998**, *26*, 1906.
44. Kosikov, K. M.; Gorin, A. A.; Lu, X.-J.; Olson, W. K.; Manning, G. S. *J. Am. Chem. Soc.* **2002**, *124*, 4838.
45. Obika, S.; Reddy, S. Y.; Bruice, T. C. *J. Mol. Biol.* **2003**, *331*, 345.
46. Ferrin, T. E.; Huang, C. C.; Jarvis, L. E.; Langridge, R. *J. Mol. Graphics* **1988**, *6*, 13.
47. Huang, C. C.; Pettersen, E. F.; Klein, T. E.; Ferrin, T. E.; Langridge, R. *J. Mol. Graphics* **1991**, *9*, 230.
48. Reddy, S. Y.; Obika, S.; Bruice, T. C. *Proc. Natl. Acad. Sci. U.S.A.* **2003**, *100*, 15475.
49. Cheatham, T. E., III; Kollman, P. A. *J. Mol. Biol.* **1996**, *259*, 434.
50. Gueron, M.; Kochoyan, M.; Leroy, J. *Nature* **1987**, *328*, 89.
51. Moe, J. G.; Folta-Stogniew, E.; Russu, I. M. *Nucleic Acids Res.* **1995**, *23*, 1984.
52. Altona, C.; Sundaralingam, M. *J. Am. Chem. Soc.* **1972**, *94*, 8205.
53. Winger, R. H.; Liedl, K. R.; Rudisser, S.; Pichler, A.; Hallbrucker, A.; Mayer, E. *J. Phys. Chem. B* **1998**, *102*, 8934.
54. Arnott, S.; Selsing, E. *J. Mol. Biol.* **1974**, *88*, 509.
55. Mocci, F.; Saba, G. *Biopolymers* **2003**, *68*, 471.
56. Grzeskowiak, K.; Yanagi, K.; Prive, G. G.; Dickerson, R. E. *J. Biol. Chem.* **1991**, *266*, 8861.